Talanta 243 (2022) 123337

Contents lists available at ScienceDirect

Talanta

journal homepage: www.elsevier.com/locate/talanta

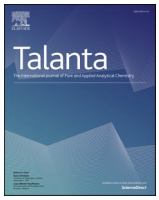

β-1,4-Galactosyltransferase-V colorectal cancer biomarker immunosensor with label-free electrochemical detection

Danilo Echeverri, Jahir Orozco *

Max Planck Tandem Group in Nanobioengineering, Institute of Chemistry, Faculty of Natural and Exact Sciences, University of Antioquia. Complejo Ruta N, Calle 67 N° 52–20, Medellín, 050010, Colombia

A R T I C L E I N F O

Keywords:
β-1,4-Galactosyltransferase-V
CRC biomarker
Immunosensor
Label-free
SAM
EIS

A B S T R A C T

β-1,4-Galactosyltransferase-V (β-1,4-GalT-V) is a membrane-bound glycoprotein with glycosyltransferase enzyme activity that synthesizes lactosylceramide and glycosylates high-branched *N*-glycans in the Golgi apparatus. Colorectal cancer (CRC) tumor cells have shown to overexpress these biomolecules concerning normal cells, releasing them into the body fluids. Thus, their detection has been suggested as a diagnosis/prognosis CRC biomarker. We report the first electrochemical immunosensor for the detection of such a novel β-1,4-GalT-V CRC biomarker. The label-free electrochemical immunosensor covalently coupled an anti-β-1,4-GalT-V antibody at a mixed self-assembled monolayer-coated screen-printed gold electrode (SPAuE) surface. This functionalized platform captured the β-1,4-GalT-V glycoprotein from human serum samples with high specificity, which response monitored by electrochemical impedance spectroscopy (EIS) was protein concentration-dependent. The resultant electrochemical immunosensor showed a linear dynamic range from 5 to 150 pM, with a sensitivity of 14 Ω pM^{-1} and a limit of detection of 7 pM, of clinical relevance. This outstanding performance makes it great potential for including it in a biomarker signature for the early diagnosis/prognosis of CRC.

1. Introduction

β-1,4-GalT-V has emerged as a candidate biomarker for diagnosing and treating human CRC [1]. β-1,4-GalT-V is a membrane-bound glycoprotein localized in the Golgi apparatus with transferase enzyme activity. It catalyzes galactosylation of glucosylceramide to synthesize the glycosphingolipid lactosylceramide [2]. β-1,4-GalT-V also catalyzes galactosylation of the *N*-acetylglucosamine β-1-6 mannose group of the highly-branched *N*-glycans [3]. There is evidence that CRC tumor cells synthesize β-1,4-GalT-V at high levels concerning normal cells [1]. Furthermore, it is widely accepted that the expression levels of different glycosyltransferases changes during carcinogenesis [4]. These glycosyltransferases can be released from the Golgi membrane after protease activity and then secreted into body fluids [5–7]. Hence, this suggests that β-1,4-GalT-V glycoprotein could be released into body fluids and used as a biomarker in CRC diagnosis [8].

Previous research reported the β-1,4-GalT-V quantification by Enzyme-Linked Immunosorbent Assay (ELISA) in CRC human tissues and mice skin [1,9]. It has also been used proteomics approaches to detect other glycoproteins and glycosyltransferases. These approaches combine liquid chromatography with mass spectrometry-based methods and data analysis by bioinformatics tools [10,11]. However, ELISA has some limitations, including laborious procedures, limited multiplexing options and requires centralized laboratory equipment, and relatively high sample volume [12]. Likewise, proteomics approaches are technically demanding and require sophisticated laboratory equipment and skilled personnel [13]. In addition, glycosyltransferases into human serum are at low levels (ng mL^{-1}) in healthy individuals concerning those diagnosed with the disease [5,14]. Therefore, sensitive, specific, simple, rapid, and precise tests must be implemented to detect the β-1,4-GalT-V both in health and disease conditions to reduce analysis time and cost and implement disease diagnosis in low- and middle-income regions with limited resources [15].

Electrochemical biosensing is a powerful tool for determining single or multiple clinical biomarkers at different molecular levels because it allows simple, rapid, affordable, and accurate determination [16]. Electrochemical biosensors have been developed using multiple bioreceptors, such as antibodies, nucleic acids, aptamers, glycans, and peptides, etc. [17–21]. Among electrochemical biosensors, immunosensors have shown great potential for real sample analysis due to their high specificity, sensitivity, accuracy, low detection limits and fast response. They can be of convenient operation, portable, amenable for

* Corresponding author.
E-mail address: grupotandem.nanobioe@udea.edu.co (J. Orozco).

https://doi.org/10.1016/j.talanta.2022.123337
Received 7 December 2021; Received in revised form 10 February 2022; Accepted 25 February 2022
Available online 3 March 2022
0039-9140/

miniaturization and cost-affordable [22]. Electrochemical biosensors interrogated by the highly sensitive Electrochemical Impedance Spectroscopy (EIS) technique excel in simplicity, enhanced limits of detection, and portability [23]. Yet, there is no single report on a β-1,4-GalT-V glycoprotein biosensor to the best of our knowledge.

This paper reports on the first electrochemical immunosensor for the determination of β-1,4-GalT-V glycoprotein. The label-free electrochemical immunosensor uses a polyclonal anti-β-1,4-GalT-V antibody as a bioreceptor that captures the analyte glycoprotein. The anti-β-1,4-GalT-V antibody was covalently immobilized onto an SPAuE, previously functionalized with a mixed self-assembled monolayer (SAM). The SAM provides available carboxylic acids for the anti-β-1,4-GalT-V antibody covalent attachment. The antibody-glycoprotein interaction was detected and quantified by EIS. The resultant immunosensor was highly specific for the β-1,4-GalT-V glycoprotein capture, detecting and quantifying it in commercial human serum samples, thus holding considerable potential for determining other proteomic biomarkers. Also, the biosensing platform simplicity, low limit of detection achieved (pM range), and label-free operation mode, attributes required for miniaturization, make this an ideal candidate immunosensing device for diseases diagnosis close to the patient.

2. Materials and methods

2.1. Reagents and solutions

11-Mercaptoundecanoic acid (MUA), 6-mercapto-1-hexanol (MCH), absolute ethanol, ethanolamine (ETA), potassium ferricyanide (III) ($K_3[Fe(CN)_6]$) and potassium hexacyanoferrate (II) trihydrate ($K_4[Fe(CN)_6]\cdot 3H_2O$) were purchased from Merck Millipore. Disodium hydrogen phosphate (Na_2HPO_4), potassium nitrate (KNO_3) and Tween-20 were acquired from PanReac AppliChem. Potassium dihydrogen phosphate (KH_2PO_4), potassium chloride (KCl) and sodium chloride (NaCl) were obtained from J.T.Baker®. Sulphuric acid (H_2SO_4) was purchased from Honeywell Fluka™. Bovine serum albumin (BSA), human serum, 2-(*N*-morpholino) ethanesulfonic acid sodium salt (MES), *N*-(3-dimethylaminopropyl)-*N*′-ethylcarbodiimide hydrochloride (EDC) and *N*-hydroxysuccinimide (NHS) were purchased from Sigma-Aldrich. Anti-β-1,4-GalT-V antibody (ab110398), recombinant β-1,4-GalT-V glycoprotein (ab160437), recombinant cellular tumor antigen (p53) protein (ab199593), anti-p53 antibody (ab28), interleukin-8 (IL-8, ab48481), and anti-human immunoglobulin (IgG) antibody (ab97161) were purchased from Abcam. All reagents were used as received and the solutions were prepared using ultrapure water of 18 MΩ cm from a Smart2Pure 3 UV/UF Milli-Q system. Phosphate Buffered Saline PBS 1X, pH 7.4 was used to prepare the antibody and glycoprotein solutions and spiked human serum samples.

2.2. Equipment and SPAuEs pretreatment

We purchased SPAuEs employed in the electrochemical measures from Metrohm DropSens (ref 220 BT). They consist of a three-electrode cell configuration with a 4 mm working gold electrode, a counter gold electrode, and a silver pseudo-reference electrode printed all together on the ceramic substrate. We performed the electrochemical measurements in a multi-channel potentiostat/galvanostat MultiPalmSens 4 with software MultiTrace version 4.4. We used SPAuEs because gold surfaces are amenable for functionalization with alkanethiols-based self-assembled monolayers (SAMs), acting as an interface to biomolecules immobilization [24–29]. Furthermore, gold is a reasonably inert material resisting oxidation (in comparison to silver), has surface defects appropriate for electron transfer, and has high electrical conductivity [30–32].

First, we cleaned the surface of the SPAuE through electrochemical activation in an acidic medium. The electrochemical activation was carried out in 0.1 M H_2SO_4 by Cyclic Voltammetry (CV). We scanned the potential between +1.6 V and 0 V (vs Ag pseudo-reference electrode) at a scan rate of 0.1 V s^{-1} for 5 cycles. When the surface of SPAuE was activated, we estimated the effective area by considering that the reductive peak from the gold surface has a charge density of 410 μC cm^{-2} [33]. Finally, we calculated the electroactive area (A) of the electrodes with the Randles-Sevcik equation, from the CV experiments in 1 mM $K_3[Fe(CN)_6]$/0.1 M KNO_3, at a scan rate of 50 mV s^{-1}. This final step was necessary to verify the proper activation of the electrode surface. See details in the supporting information (SI) section.

2.3. Electrochemical measurements

We characterized the biosensing platform by electrochemical techniques. At each step of the immunosensor assembly, we evaluated the electrochemical performance by CV and EIS using the redox pair 5 mM $[Fe(CN)_6]^{4-/3-}$ in PBS 1X pH 7.4 as supporting electrolyte. The potential window for CV was between +0.5 V and −0.1 V, at a scan rate of 0.05 V s^{-1} for 3 consecutive cycles. This measurement was made initially with the bare electrode and later after each step of the functionalization process. To carry out the EIS measurement, we applied the formal potential of the redox pair (+0.18 V). The amplitude of the sinusoidal wave was 10 mV and frequencies ranging from 100 kHz to 0.1 Hz. We held the potential for 1 min before recording each spectrum to ensure the system reached a steady-state condition [34,35]. We fitted the EIS data to the electrical equivalent circuit using EIS analyzer software to characterize the interfacial electrical properties.

We performed the impedance measurements after each step of the immunosensor development, i.e., after the formation of the mixed SAM, activation of the carboxyl groups, covalent coupling of the antibody, blocking off the remaining active esters, and incubation with the molecular target.

We used the electrical equivalent circuit R_s (CPE R_{ct}) to model the SAM formation step for data analysis. Subsequent steps were fitted to R_s (CPE [R_{ct} Z_w]), where R_s is the solution resistance, CPE is the constant phase element, R_{ct} the charge transfer resistance and Z_w the Warburg's element.

2.4. Assembly of the electrochemical immunosensor

We started the assembly of the electrochemical immunosensor by forming a mixed SAM of alkane-thiols through chemisorption onto the SPAuE surface. It enables functionalization of the electrode surface with carboxylic groups placed distal to the thiol group of the SAMs. For achieving it, we submerged the SPAuE in an ethanolic solution containing a mixture of a 1:1 M ratio of MUA and MCH at a concentration of 1 mM for 30 min. After incubation, we washed the SPAuEs with absolute ethanol and finally with ultrapure water [26].

Once a SAM was formed with carboxyl and hydroxyl groups on the SPAuE surface, we proceeded with the anti-β-1,4-GalT-V antibody covalent coupling. We used the EDC-NHS chemistry to activate the carboxyl group of MUA on the SPAuE surface. To achieve this, we added 4 μL of a 400 mM EDC and 100 mM NHS mixture, prepared in a 25 mM MES buffer solution pH 6.5, for 15 min. At the end of this step and in the following incubation steps, the SPAuE was washed with ultrapure water. Next, we added 6 μL of 40 μg mL^{-1} anti-β-1,4-GalT-V antibody solution prepared in PBS 1X pH 7.4 for 90 min, and later we blocked the remaining active esters with 1 M ethanolamine pH 8.5 for 15 min.

We used the assembled electrochemical immunosensor to detect the β-1,4-GalT-V glycoprotein by EIS. To do this, we prepared a 16 nM (722 ng mL^{-1}) β-1,4-GalT-V glycoprotein solution from a 100 μg mL^{-1} (MW 45.13 kDa) stock solution by diluting in PBS 1X pH 7.4. Next, we incubated the electrochemical immunosensor with 6 μL of the β-1,4-GalT-V glycoprotein solution for 45 min. Finally, we washed the SPAuE with ultrapure water and carried out the EIS measurement using the redox pair $[Fe(CN)_6]^{4-/3-}$ in PBS 1X pH 7.4 as an electrochemical probe and supporting electrolyte, respectively.

2.5. Optimization of experimental parameters

Once we confirmed the functionality of the electrochemical immunosensor, we optimized the anti-β-1,4-GalT-V antibody concentration based on the best signal/noise (S/N) ratio. The S/N ratio was calculated as the ratio between R_{ct} (β-1,4-GalT-V) and R_{ct} (ETA), where R_{ct} (β-1,4-GalT-V) was the charge transfer resistance value related to the binding of β-1,4-GalT-V glycoprotein to the antibody and R_{ct} (ETA) was the charge transfer resistance value having the anti-β-1,4-GalT-V antibody immobilized on the SPAuE surface and remanent reactive esters blocked with ETA. In this assay, we evaluated anti-β-1,4-GalT-V antibody concentrations of 5, 10, 20, 40, and 50 μg mL^{-1} at excess of β-1,4-GalT-V glycoprotein concentration (16 nM, 722 ng mL^{-1}) for 45 min and chose the concentration at which the S/N ratio was the largest. Therefore, we selected this concentration for the following experiments (optimization of the β-1,4-GalT-V glycoprotein incubation time with the immunosensor and building the calibration curve). Finally, we evaluated β-1,4-GalT-V glycoprotein incubation times with the immunosensor from 15 to 60 min and chose the time with the highest S/N ratio.

2.6. Determination of analytical parameters

Once we determined the optimal conditions, we evaluated the analytical performance of the electrochemical immunosensor, detecting different concentrations of the β-1,4-GalT-V glycoprotein. Different dilutions with known β-1,4-GalT-V glycoprotein concentrations were evaluated by EIS using the difference in charge transfer resistance (ΔR_{ct}) as the response variable for β-1,4-GalT-V glycoprotein quantification. The biosensor calibration curve was made by plotting ΔR_{ct} versus β-1,4-GalT-V glycoprotein concentration. Changes in resistance were calculated according to $\Delta R_{ct} = R_{ct}$ (β-1,4-GalT-V) - R_{ct} (ETA). Proper volumes of β-1,4-GalT-V glycoprotein stock solution were diluted up to 100 μL of buffer PBS 1X pH 7.4 to get 5, 50, 75, 100 and 150 pM (0.23, 2.26, 3.38, 4.51 and 6.77 ng mL^{-1}). Finally, we analyzed the resulting β-1,4-GalT-V glycoprotein solutions with three independent immunosensors. We determined the limit of detection (LOD) and the limit of quantification (LOQ) of the biosensor by using the 3-sigma and 10-sigma criteria, respectively, with $LOD = 3S_b/m$ and $LOQ = 10S_b/m$, where S_b is the standard deviation for the R_{ct} (ETA), and m is the slope of the calibration curve.

2.7. Specificity and selectivity studies

To assess the specificity of the electrochemical immunosensor, we evaluated the cross-reactivity of the anti-β-1,4-GalT-V antibody separately to p53 protein, anti-p53 antibodies, IL-8 and IgG. Such biomolecules are overexpressed in CRC tumors and could be cross-reactive with the anti-β-1,4-GalT-V antibody. IgG is an abundant biomolecule in human serum and could also interfere with the determination of β-1,4-GalT-V. The concentration evaluated of p53, anti-p53, IL-8, and IgG was 50 μg mL^{-1}. The selectivity was assessed by mixing 10 μg mL^{-1} of p53, anti-p53, IL-8, and IgG in a buffer PBS 1X pH 7.4 containing 100 pM (4.51 ng mL^{-1}) β-1,4-GalT-V glycoprotein. Finally, we completed these analyses using the protocol mentioned above to detect the β-1,4-GalT-V glycoprotein by EIS. We performed a paired *t*-test and a 1-way ANOVA with a level of statistical significance of 99% to evaluate the statistical significance between the samples.

2.8. Quantification of β-1,4-GalT-V glycoprotein in human serum

As a proof of concept, we used the electrochemical immunosensor to detect the β-1,4-GalT-V glycoprotein in commercial human serum. First, we spiked 10 μL of human serum with known concentrations of β-1,4-GalT-V glycoprotein (2.5, 5.0, 7.5 and 1.0 nM) and next diluted the spiked serum 1:100 with PBS pH 7.4 containing 0.1% Tween-20 (v/v) and 3% BSA (w/v). The resultant solutions were vortexed for 15 s and incubated at 37 °C for 15 min to dissolve the possible lipid aggregates present in the matrix. We removed the insoluble residual components of the sample by centrifugation at 13,000 rpm, 4 °C for 5 min. After that, we dropped 4 μL of supernatant onto the SPAuE and incubated it in the humidity chamber for 30 min to bind the β-1,4-GalT-V glycoprotein. We performed a series of washing steps with ultrapure water to remove the components that did not bind to the antibody. Finally, we completed these analyses using the protocol mentioned above to detect the β-1,4-GalT-V glycoprotein by EIS.

We also detected the β-1,4-GalT-V glycoprotein in undiluted serum. For this purpose, we spiked human serum with known concentrations of β-1,4-GalT-V glycoprotein (25, 50, 75, and 100 pM) and dropped 6 μL of undiluted serum samples onto the SPAuE. After a series of washing steps with ultrapure water, we completed these analyses using the protocol mentioned above to detect the β-1,4-GalT-V glycoprotein by EIS.

3. Results and discussion

3.1. Development of the electrochemical immunosensor

We successfully developed a label-free electrochemical immunosensor for the detection of β-1,4-GalT-V glycoprotein, as shown in Scheme 1. For this purpose, we assembled the immunosensor, step by step, starting with forming a mixed MUA/MCH SAM onto the SPAuE surface. The SAM formation was followed by chemical activation of carboxylic acids with EDC/NHS, forming a reactive *N*-hydroxysuccinimidyl ester (NHS-ester) on the SPAuE surface. After activation of carboxylic acids, we attached the anti-β-1,4-GalT-V antibody by amide bond formation between the NHS-ester onto the SPAuE surface and primary amine groups from the antibody. Following anti-β-1,4-GalT-V antibody covalent attachment on the SPAuE surface, we reverted unreacted NHS-esters with ethanolamine, preventing the non-specific binding of proteins onto the SPAuE surface.

The anti-β-1,4-GalT-V antibody attached to the surface of SPAuE was the bioreceptor that specifically and selectively recognized the target glycoprotein. The immunosensor's working principle was the molecular interaction between anti-β-1,4-GalT-5 antibody with β-1,4-GalT-V glycoprotein by an antigen-antibody affinity reaction. When the antibody captured the target glycoprotein on the electrode surface, the interfacial electrical properties were disturbed. Then, the electrochemical transducer detected these changes in interfacial electrical properties and transferred the output signal from the molecular biochemical domain to the electrical domain into quantitative analytical information. Finally, the electrical signal was correlated to the glycoprotein concentration.

3.2. Functionalization of the SPAuE surface

The immunosensor functionalization required self-assembly and molecularly well-ordered alkanethiols immobilization onto a solid-state conductive SPAuE surface [36]. To achieve it, we used a mix of alkanethiols consisting of MUA and MCH; the SAM was formed by spontaneous chemisorption of these alkanethiols onto the SPAuE surface. This chemisorption led to well-defined packed and dense MUA and MCH in a molecular layer on the SPAuE surface, with free carboxylic acids available for antibody coupling from the solution phase [37,38]. The chemisorption needed to be controlled and reproducible to achieve proper immunosensors reproducibility and repeatability by activating the SPAuE by CV in acidic conditions [39]. This CV was used to obtain the voltammograms corresponding to the gold reduction and oxidation processes, as shown in S.I. Figure S1A. The resultant voltammogram enabled calculating the effective area (A_e) by integrating the gold oxide reduction peak in the last scan (5th cycle) and using a value of 410 μC cm^{-2} as the corresponding charge required for the reduction of gold oxide monolayer to consider the SPAuE surface roughness [39]. Such surface defects generate heterogeneity of the surface energy states,

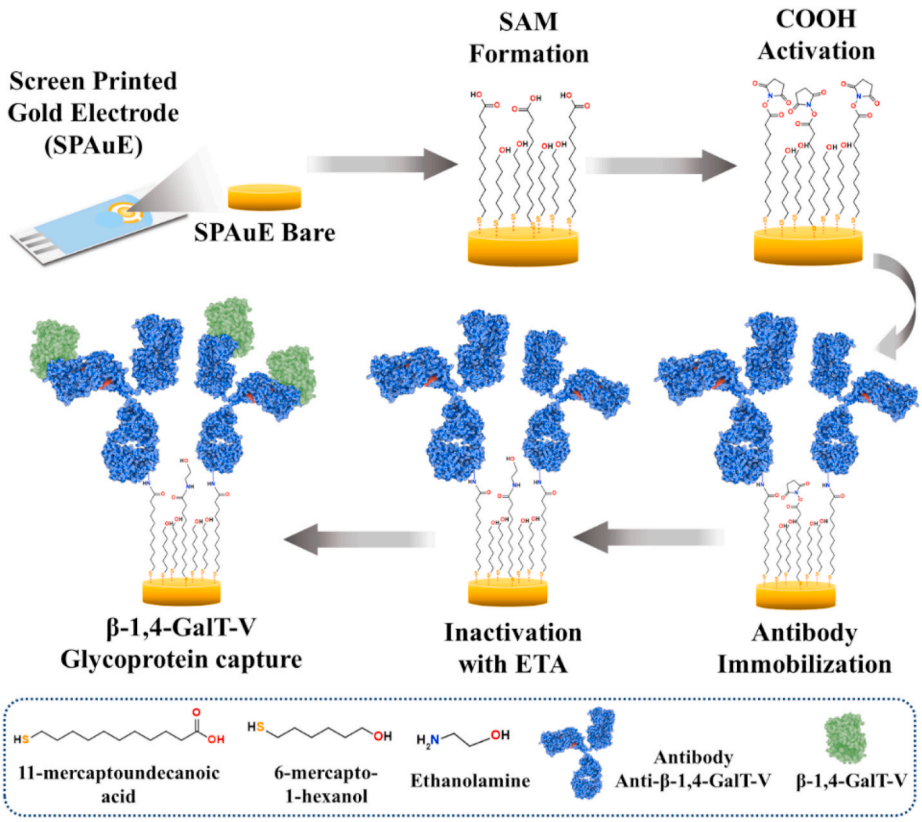

Scheme 1. Assembly steps of the electrochemical immunosensor. 1) Self-assembled monolayer formation. 2) Carboxylic acids activation. 3) Antibody covalent immobilization. 4) Reverting remanent NHS-esters. 5) Glycoprotein capture.

where current could pass through depending on the phase boundary [40]. The calculated A_e from CV data was 126.5 ± 4.4 mm^2, more significant than the geometric area. Once A_e was calculated, we maintained the surface roughness factor (A_e/A_g) at 10 ± 0.3 to get a reproducible SAM on the SPAuE surface, considering $A_g = 12.6$ mm^2 as the geometric area reported by the manufacturer.

We then calculated an electroactive area (A) of 12.5 ± 0.05 mm^2, closed to A_g, using the Randles-Sevcik equation from CV experiments in 1 mM K_3 [$Fe(CN)_6$]/0.1 M KNO_3, at 50 mV s^{-1} (S.I. Figure S1B) [41]. The electroactive area represented the SPAuE surface area accessible to the electrochemical probe for the redox process [42]. These results indicate the proper activation of the SPAuEs with an interelectrode relative standard deviation lower than 3% in ten independent SPAuEs. Afterward, the SPAuEs were treated with the MUA/MCH solution, and the SAM was formed successfully and reproducibly onto the SPAuE surface. SPAuEs have a high surface roughness that may decrease the quality of monolayer assembly and molecular packing [36,43]. However, although the SAM is less ordered and packed, the 11-MUA enables an efficient immobilization of antibodies onto the electrode surface, and therefore, a high antigen binding [44].

3.3. Electrochemical characterization of the immunosensor

Each step of immunosensor' assembly was electrochemically characterized by CV and EIS using 5 mM $Fe(CN)_6^{4-/3-}$/PBS 1X as a redox probe, as shown in Fig. 1A. The maximum current intensity corresponds to the bare SPAuE because the redox probe diffused to the SPAuE surface without steric hindrance and, therefore, with fast electron transfer kinetics. After SAM formation on the SPAuE surface, the current intensity decreased drastically due to electrostatic repulsion between the MUA's carboxylic acids onto the SPAuE surface and the redox probe in solution [45]. Once carboxylic acids were activated, the current intensity increased because *N*-hydroxysuccinimidyl ester (NHS-ester) is an uncharged compound; therefore, the electrostatic repulsion between the redox probe and SPAuE surface decreased, promoting the reduction and oxidation reactions [46]. Contrarily, the antibody attached to the SPAuE surface hindered electron transfer, dropping the current intensity. After blocking unreacted NHS-esters, we observed that current intensity increased because the deactivation of unreacted NHS-esters with ethanolamine decreased electrostatic repulsion and promoted electron transfer.

The results obtained with CV showed how the interfacial electrical properties changed as the immunosensor assembled. However, these interfacial electrical changes were more evident when characterized by EIS; with this technique, significant changes in charge transfer resistance were observed after each immunosensor assembly step, as shown in Fig. 1B. The interfacial electrical changes were evidence of successful biomolecules immobilization onto the SPAuE surface. These biomolecules immobilized onto the SPAuE surface hindered the electron transfer from the soluble redox probe to the SPAuE surface, increasing the R_{ct}. The electrochemical process on the SPAuE surface was modeled by the electrical equivalent circuit depicted in Fig. 1B (inset), where R_s is the electrolyte solution resistance, R_{ct} is the charge transfer resistance, *CPE* is the constant phase element, and Z_w is the Warburg's element. The electrical equivalent circuit was used to quantify each electrical element that described the electrochemical characteristics of the SPAuE/electrolyte interface. The SPAuE surface in the electrolyte had capacitive (*CPE*) and solvent resistive (R_s) contributions, modeled by R_s in series with *CPE*. We used the *CPE* instead of the typical double-layer capacitance (C_{dl}) to consider the interfacial heterogeneity of the SPAuE surface that depends on a pre-exponential factor (*P*) and an exponent (*n*) [47]. The values obtained for *P* indicated a decrease in the capacitive component of the system as the R_{ct} increased and the *n* values were less than one, consistent with a pseudo interfacial double layer capacitance

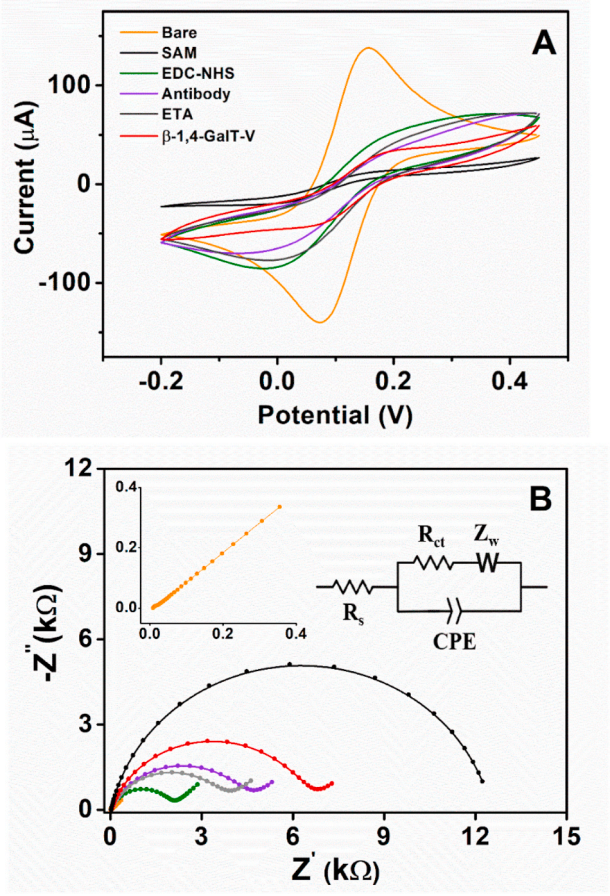

Fig. 1. (A) Cyclic voltammograms for each immunosensor's assembly step at a scan rate of 50 mV s^{-1} (the bare electrode is in the inset). (B) Nyquist plot with frequency range 100 kHz to 0.1 Hz, amplitude 10 mV (the bare electrode and the electrical equivalent circuit are in the inset). The redox probe was 5 mM $[Fe(CN)_6]^{4-/3-}$/PBS 1X, pH 7.4.

at the SPAuE/electrolyte interface [48]. Furthermore, the presence of the soluble redox probe added two additional components into the equivalent circuit, i.e., R_{ct}, describing electron transfer kinetics, and Z_w describing diffusional resistance for the redox probe [23]. We calculated R_{ct} from the impedance spectra visualized as Nyquist plot (Fig. 1B), which allowed calculating R_{ct} from the diameter of the semicircle. On the other hand, Z_w corresponded to the straight line in the low-frequency range of the Nyquist plot. The specific molecular binding on the SPAuE surface altered the interfacial electrical properties, and one or more of the electrical equivalent circuit elements changed (significantly R_{ct}). By this, we used R_{ct} to detect the molecular binding between the antibody and glycoprotein on the SPAuE surface.

The results of the electrochemical characterization by EIS are shown in Fig. 1B, the Nyquist plot for each step of the immunosensor' assembly. Fig. 1B inset shows the Nyquist plot from the bare SPAuE, which presented a typical trend of a conductive surface, where the charge transfer resistance was low ($R_{ct} = 94 \pm 20$ Ω) and the electrochemical reaction kinetics was controlled by probe diffusion. After SAM formation onto the SPAuE surface, Nyquist plot semicircle diameter increased significantly, indicating a greater hindering to electron transfer ($R_{ct} = 12{,}517 \pm 62$ Ω). This result was attributed to the electrostatic repulsion between carboxylic acids on the SPAuE surface and the negatively charged probe. In contrast, once carboxylic acids were activated, the electrostatic repulsion decreased, and a drop in R_{ct} was observed down to 1804 ± 106 Ω. The covalent attachment of the antibody on the SPAuE surface increased the R_{ct} to 4501 ± 91 Ω because this biomolecule hindered the electron transfer from the redox probe. This increase in R_{ct} indicated the successful attachment of the antibody on the SPAuE surface. Once the antibody was immobilized onto the SPAuE surface, reverting the remaining activated esters with ethanolamine reduced the negative charges and introduced hydrophilic groups, producing a slight drop in R_{ct} to 4208 ± 34 Ω.

Finally, we evaluated the R_{ct} after the antibody-glycoprotein interaction. When the antibody recognized the glycoprotein by a biochemical affinity reaction, it was observed a significant increase in R_{ct} from 4208 ± 34 Ω up to 6465 ± 50 Ω. This result indicates the successful molecular biorecognition event between antibody and glycoprotein, which hindered the electron transfer at the SPAuE/electrolyte interface. In addition, we normalized the CV and EIS results when developing the biosensing platform to the surface area to facilitate comparison with other laboratories regardless of the electrodes. (see S.I. Figure S2). The values of the Chi-squared function (χ^2) were lower than 4.6×10^{-3}, which indicated a proper fitting of experimental data and the electrical equivalent circuit (see S.I. Figure S3). Table 1 summarizes all fitted circuit elements mentioned above. It is important to highlight that the SAM completely blocked the SPAuE surface so that the Nyquist plot lacks Warburg's diffusion. Therefore, to model the SAM on the SPAuE surface, the electrical equivalent circuit did not include Warburg's element. Remarkable, we achieved high inter-electrode reproducibility because the relative standard deviation (RSD) for R_{ct0} of 5 and 10 immunosensors was 2.21 and 4.60%, respectively.

3.4. Optimization of experimental parameters

In seeking to optimize the immunosensor performance, we considered two experimental parameters regardless of the antibody bioreceptor. First, we evaluated different antibody concentrations intending to generate an antibody density high enough to maximize the glycoprotein capture probability but low enough to avoid steric hindrance effects on the electrode surface [49]. The EIS responses and ΔR_{ct} calculated for each antibody concentration are shown in Fig. 2A–E and Fig. 2F, respectively. Because we used independent electrodes for each antibody concentration, the starting value of R_{ct0} is different for each electrode. The R_{ct0} reached a maximum value when antibodies molecules saturated the electrode surface [50,51]. The best S/N = 1.54 and most significant ΔR_{ct} was observed by antibody covalent attachment at 40 μg mL^{-1}. At this concentration, a higher antibody loading was attached to the SPAuE surface and maximized the probability of capturing the glycoprotein, selected as optimal. Next, we evaluated the effect of glycoprotein incubation time at 40 μg mL^{-1} antibody. The effects of glycoprotein incubation time on the EIS responses and

Table 1
Electrochemical characterization of the biosensor. Data from EIS experiments. Charge-transfer resistance (R_{ct}), electrolyte solution resistance (R_s), Warburg impedance (Z_W), constant phase element (*CPE*) with pre-exponential factor (P) and exponent (n) and Chi-squared function (χ^2).

[β-1,4-GalT-V][a]	R_{ct} (kΩ)	R_s (Ω)	Z_W (Ω $s^{-0.5}$)	*CPE*		χ^2
				P (Ω^{-1} s^n)	n	
SPAuE bare	0.09 ± 0.02	25 ± 1	827 ± 46	8.98×10^{-5}	0.7	6.49×10^{-4}
SAM MUA/MCH	12.52 ± 0.06	24 ± 1		1.25×10^{-5}	0.9	2.82×10^{-3}
EDC/NHS	1.80 ± 0.11	26 ± 2	230 ± 2	3.74×10^{-5}	0.8	3.81×10^{-3}
Antibody	4.50 ± 0.09	29 ± 2	322 ± 44	1.61×10^{-5}	0.8	2.73×10^{-3}
Antibody-ETA	4.21 ± 0.03	30 ± 2	296 ± 56	2.14×10^{-5}	0.8	3.81×10^{-3}
β-1,4-GalT-V	6.46 ± 0.05	29 ± 1	339 ± 88	1.94×10^{-5}	0.8	4.61×10^{-3}

[a] 16 nM (722 ng mL^{-1}).

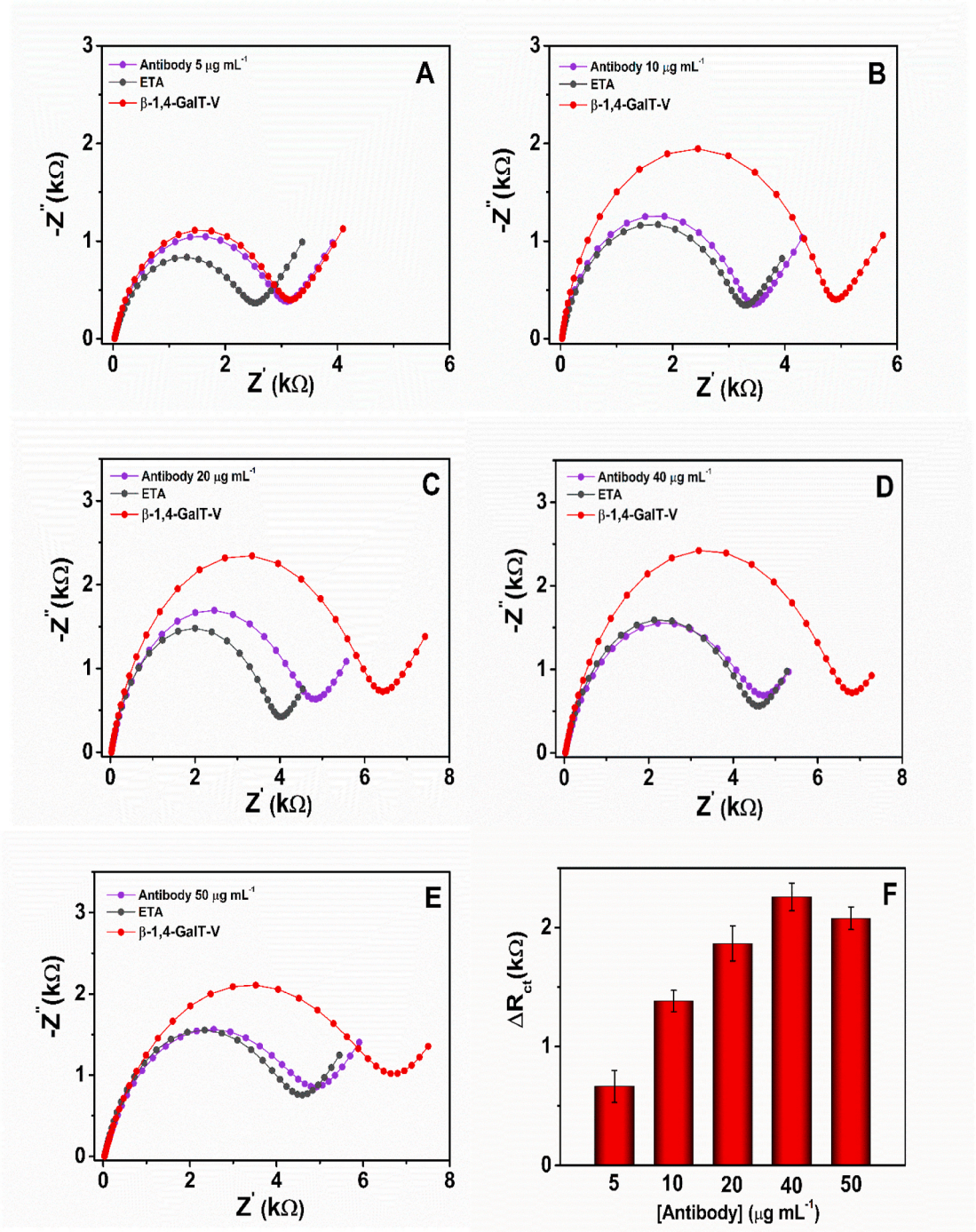

Fig. 2. Nyquist plots recorded using the redox probe 5 mM $[Fe(CN)_6]^{4-/3-}$/PBS 1X, pH 7.4, frequency range from 100 kHz to 0.1 Hz and amplitude 10 mV [Antibody]: (A) 5, (B) 10, (C) 20, (D) 40, and (E) 50 μg mL^{-1}, (F) Difference in the charge transfer resistance for the different antibody concentrations.

corresponding ΔR_{ct} are shown in Fig. 3A–D and Fig. 3E, respectively. The results showed that the ΔR_{ct} response increased as the incubation time from 15 to 30 min, with a maximal S/N ratio of 1.66 at 30 min; then ΔR_{ct} response decreased, suggesting that the formation of the antibody-glycoprotein complex has reached a saturation level on the SPAuE surface [52]. Therefore, 30 min was selected as the optimal incubation time for the glycoprotein detection. Finally, we used the optimal 40 μg mL^{-1} glycoprotein for 30 min in subsequent experiments to assess the immunosensor analytical performance.

3.5. Analytical parameters and calibration curve

Once we determined optimal conditions for glycoprotein detection, we assessed the immunosensor analytical performance by analyzing different solutions containing known concentrations of β-1,4-GalT-V ranging from 5 pM to 16 nM (0.23–722 ng mL^{-1}). We built a calibration curve by estimating the ΔR_{ct} for each resultant glycoprotein solution, as shown in Fig. 4. This figure evidenced that R_{ct} did not change at a concentration above 150 pM due to saturation, allowing us to determine the immunosensor linear range. The data showed a linear correlation of ΔR_{ct} with the β-1,4-GalT-V glycoprotein concentration in the range from 5 to 150 pM (0.23–6.77 ng mL^{-1}) as described by the equation ΔR_{ct} =

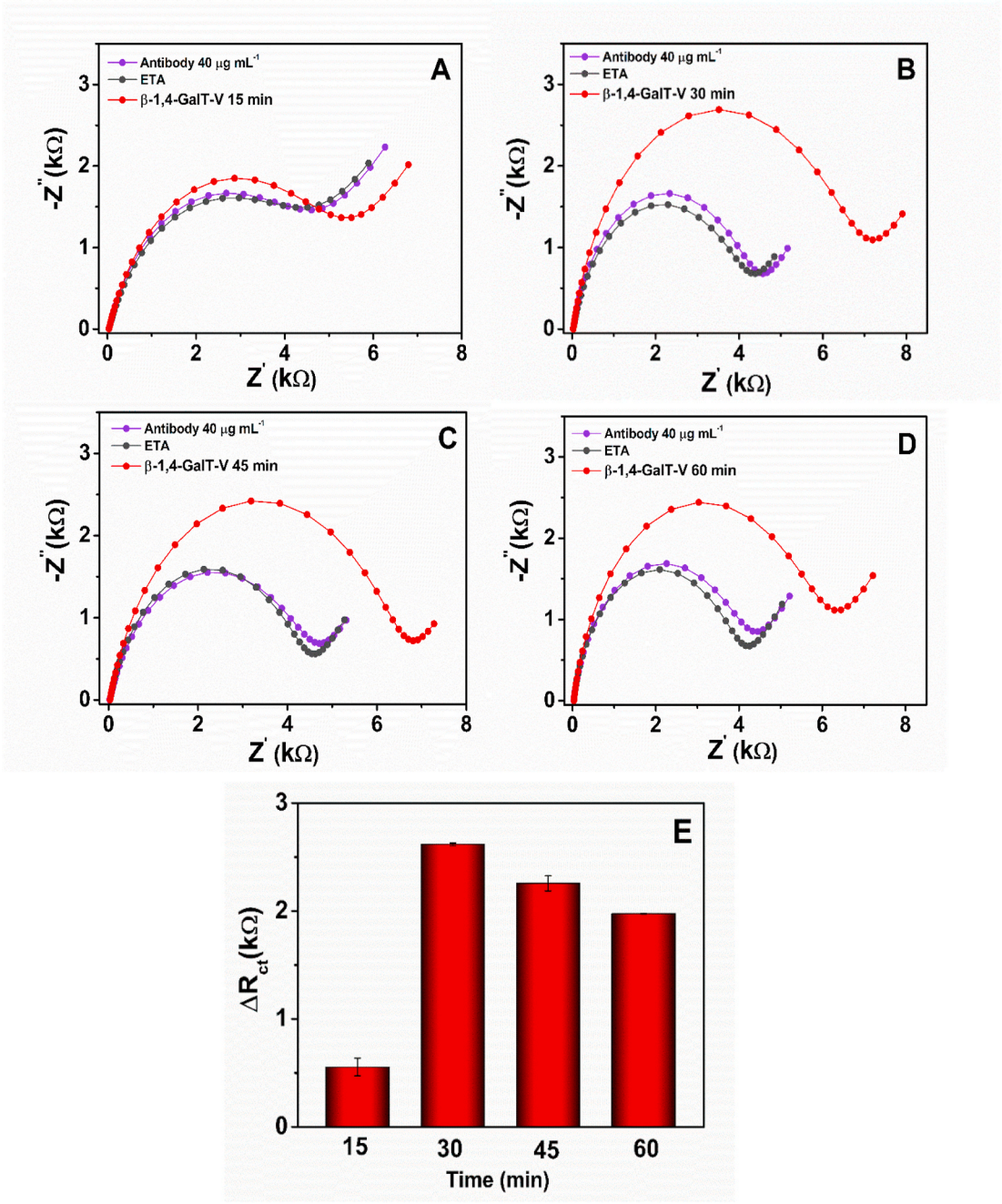

Fig. 3. Nyquist plots recorded using the redox probe 5 mM $[Fe(CN)_6]^{4-/3-}$/PBS 1X, pH 7.4, frequency range from 100 kHz to 0.1 Hz and amplitude 10 mV. Incubation times: (A) 15, (B) 30, (C) 45 and (D) 60 min. (E) Difference in the charge transfer resistance for the different incubation times.

13.96*[β-1,4-GalT-V] + 200.74 with a correlation coefficient R^2 = 0.993 (Fig. 4B). Moreover, the calculated LOD value of the immunosensor was 7 pM (0.32 ng mL^{-1}) and the LOQ 24 pM (1.08 ng mL^{-1}). From levels of β-1,4-GalT-V reported in solid tissue and quantification by ELISA, we estimated a background around 500 ng mL^{-1} [1,9] in healthy individuals. Therefore, our immunosensor could be applied to detect β-1,4-GalT-V glycoprotein in body fluids with minimally invasive procedures, according to glycoprotein levels of clinical relevance reported in the literature.

The level of β-1,4-GalT-V glycoprotein measured in protein extraction from colon tissue of healthy individuals is around 500 ng mg^{-1} with a marked increase of approximately 6.5-fold in CRC patients. Furthermore, β-1,4-GalT-V immunostaining of the cytoplasm, both in control and CRC tumor tissues, suggested that β-1,4-GalT-V must exist in a membrane-bound and a soluble form in various body fluids [1]. Furthermore, according to the ELISA method reported by Bedja et al. for the β-1,4-GalT-V quantification in tissues, we estimate that β-1,4-GalT-V concentration in fluids from healthy individuals is around 500 ng mL^{-1} [9]. There are also other reports of glycosyltransferases sera levels, which are in the range of ng mL^{-1}. The sera level of β-1,3-GalT-II galactosyltransferase in patients diagnosed with CRC has been reported to be 48 ng mL^{-1}, more significant concerning the normal level of 14 ng mL^{-1} in healthy individuals [14]. On the other hand, the sera level of β-1,3-GalT-4/5 from patients with various types of uterine cancer has been reported to have a cut-off value of 5.4 ng mL^{-1} [5]. Hence, this suggests that β-1,4-GalT-V glycoprotein could be released into the body fluids at levels ranging from pg mL^{-1} to ng mL^{-1}. These reports show that our immunosensor has the proper LOD and LOQ to detect

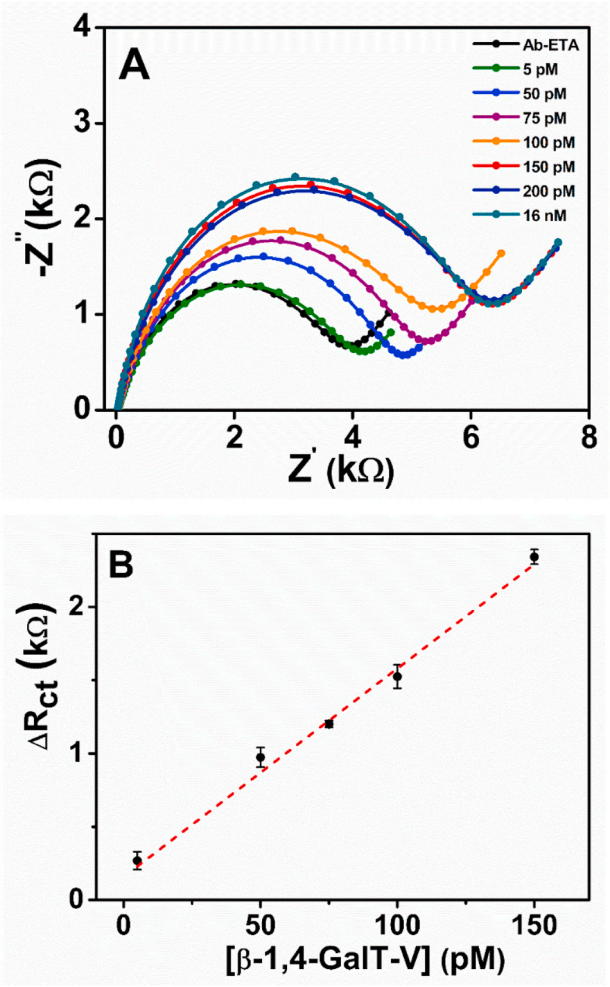

Fig. 4. (A) Nyquist plots for different glycoprotein concentrations (pM) recorded with the redox probe 5 mM $[Fe(CN)_6]^{4-/3-}$/PBS 1X, pH 7.4, frequency range from 100 kHz to 0.1 Hz and amplitude 10 mV. (B) Resultant calibration curve, with the difference in charge transfer resistance as a response variable.

glycosyltransferases at levels of clinical interest with high accuracy. Moreover, our immunosensor has a LOD and linear range similar to the commercial ELISA kits, as shown in Table S2 of the supporting information. These results suggest that it would be possible to use the immunosensor in real clinical applications with the portability offered by electrochemical biosensors. On the other hand, the sensitivity of the immunosensor could improve by incorporating conductive nanomaterials on the electrode surface. The high surface area of nanomaterials enables the immobilization of many bioreceptors, and conductive properties improve the electrochemical performance, resulting in better immunosensor sensitivity, lowering the LOD and LOQ [53]. Additionally, continuous monitoring of β-1,4-GalT-V concentration over time would be possible by differential electrochemical impedance spectroscopy (DEIS). In this approach, the EIS spectra are obtained at different times until the system reaches saturation [54]. DEIS allows the detection of tiny concentration changes within the linear range of the biosensor.

3.6. Immunosensor specificity, repeatability, and reproducibility

To assess the immunosensor specificity, we evaluated the ΔR_{ct} response to biomolecules that could cross-react with the anti-β-1,4-GalT-V antibody. The biomolecules evaluated were p53, anti-p53 antibody, IL-8 and IgG. The p53 antigen, anti-p53 antibody, and IL-8 are biomarkers overexpressed during CRC progression and are released from tumor cells to body fluids [55]. IgG is the most abundant antibody in human blood and is generally produced in response to protein and polysaccharides antigens [56]. All these biomolecules could potentially interact with the anti-β-1,4-GalT-V antibody, producing a false-negative result. Fig. 5. shows the Nyquist plot from the EIS measurements and the corresponding ΔR_{ct}. As mentioned above, these experiments used different sensor electrodes with high inter-electrodes reproducibility (RSD of $R_{ct0} = 2.44\%$). The results shown that the ΔR_{ct} was higher for the β-1,4-GalT-V glycoprotein ($\Delta R_{ct} = 1525 \pm 80\ \Omega$) compared to p53 ($\Delta R_{ct} = 69 \pm 5\ \Omega$), anti-p53 antibody ($\Delta R_{ct} = 99 \pm 26\ \Omega$), IL-8 ($\Delta R_{ct} = 127 \pm 60\ \Omega$), and IgG ($\Delta R_{ct} = 283 \pm 22\ \Omega$). The ΔR_{ct} shows a differential response with significant statistical differences when analyzed by a paired *t*-test and a 1-way ANOVA with a level of statistical significance of 99%. Yet, the slight cross-reactivity between IgG and anti-β-1,4-GalT-V antibody indicates a slight interaction between these biomolecules. This cross-reactivity can be explained by the fact that IgG antibodies could interact with the light chains and the Fc regions of the anti-β-1,4-GalT-V antibody [57]. Furthermore, when we interrogated the β-1,4-GalT-V glycoprotein in the presence of the other biomolecules, a slight increase in ΔR_{ct} was observed ($\Delta R_{ct} = 1798 \pm 124\ \Omega$). This result was attributable to slight cross-reactivity with the IgG antibody.

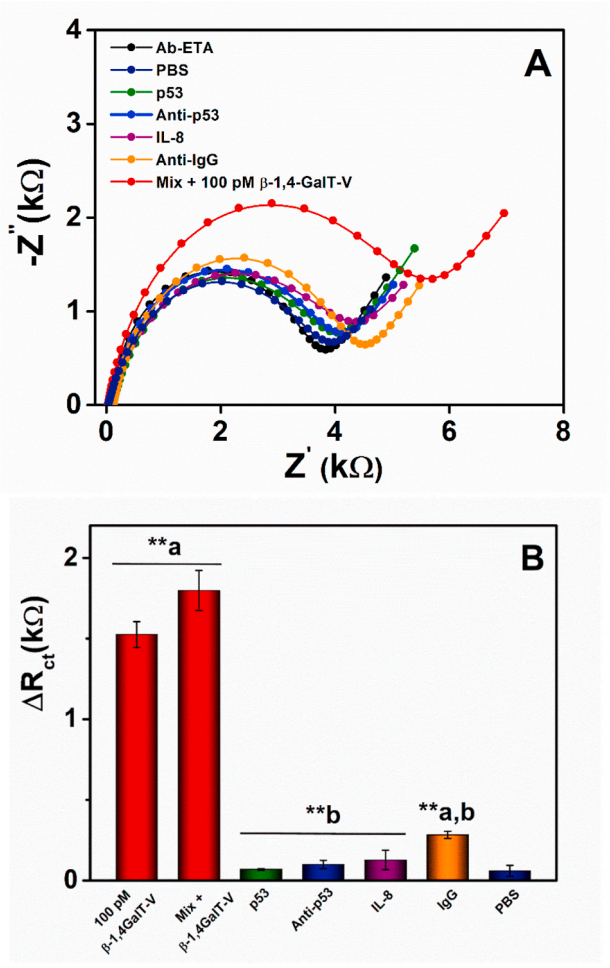

Fig. 5. (A) Nyquist plot for 100 pM β-1,4-GalT-V in the presence of 10 μg mL^{-1} p53 antigen, anti-p53 antibody, IL-8, and IgG (red curve). It also shows the EIS response for each biomolecule regardless, measured with independent immunosensors. (B) The difference in the charge transfer resistance for each sample. **a Significantly different concerning the PBS sample ($p < 0.01$). **b Significantly different respect to the 100 pM β-1,4-GalT-V sample ($p < 0.01$). (For interpretation of the references to color in this figure legend, the reader is referred to the Web version of this article.)

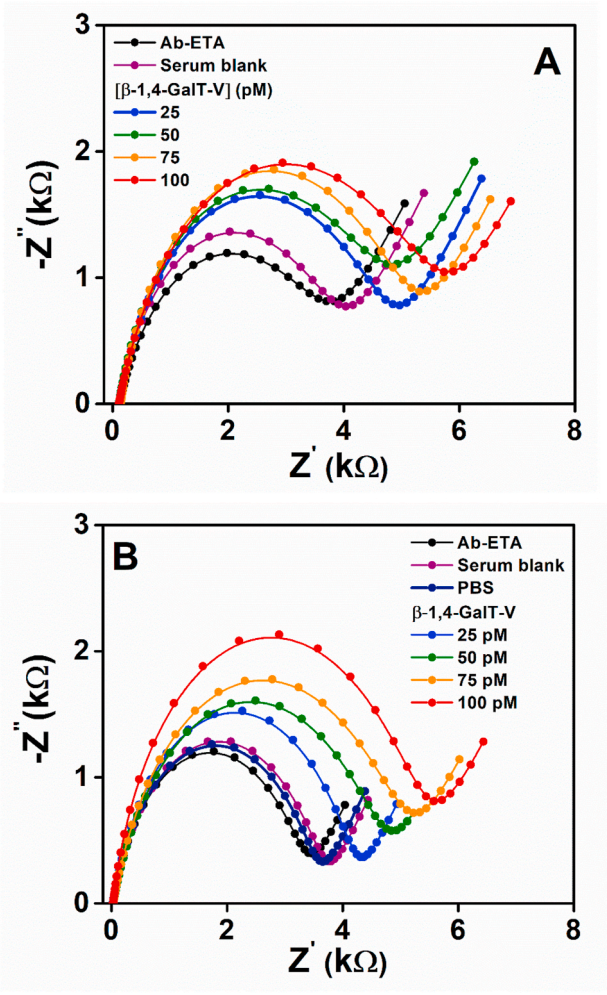

Fig. 6. (A) Nyquist plots for different glycoprotein concentrations (pM) spiked in 100-fold diluted human serum. (B) Nyquist plots for low, medium, and high glycoprotein concentrations (pM) spiked in undiluted human serum.

We evaluated the repeatability and reproducibility of our immunosensor by measuring the EIS response to 75 pM of β-1,4-GalT-V glycoprotein. The repeatability and reproducibility, calculated as relative standard deviation (RSD), were 2.1% (n = 3) and 2.7% (n = 5), respectively. Although different strategies have been reported to regenerate the SPAuE surface [58,59], we did not reuse the SPAuE to avoid changes in the electrical properties at the transducer surface that may be detected by the highly sensitive EIS over regeneration cycles. Furthermore, some studies report that SAMs have limited long-term stability, for instance, when immersed in PBS or biological media for long periods [60–63]. Because to evaluate the long-term stability is necessary to immerse the biosensors in PBS to preserve the biological activity of the antibodies, we used freshly prepared immunosensors to avoid significant changes in the EIS response.

3.7. Quantification of β-1,4-GalT-V glycoprotein in spiked human serum

To assess the possible detection of β-1,4-GalT-V glycoprotein in body fluids from a real-like sample, we spiked commercial sera samples with the β-1,4-GalT-V glycoprotein at different concentrations and implemented a sample pretreatment protocol as detailed in the Materials and methods section. The β-1,4-GalT-V glycoprotein concentration was calculated by extrapolating the ΔR_{ct} values obtained for each serum sample in the calibration curve depicted in Fig. 4B. Table 2 shows the results for the recovery assay from human sera spiked with the β-1,4-GalT-V glycoprotein. The quantity of β-1,4-GalT-V glycoprotein recovered from 100-fold diluted sera was ~100% for concentrations from 50 to 100 pM. At a concentration of 25 pM, the quantity recovered of β-1,4-GalT-V glycoprotein was the lowest (~84%). This result may be explained by the fact that the LOQ of the immunosensor is 24 pM, which is a close value to the concentration tested and the matrix effect may be considerable [64–66]. Nevertheless, the results showed that the immunosensor enabled the β-1,4-GalT-V glycoprotein detection in spiked human serum with high accuracy.

Table 2
Recovery assay in human serum spiked with β-1,4-GalT-V glycoprotein.

Diluted sera [β-1,4-GalT-V] (pM)[a]	ΔR_{ct} (kΩ)	Recovered [β-1,4-GalT-V] (pM)	Recovery (%)	RSD (n = 3) (%)
Blank	0.23 ± 0.06	N.D		
25	0.72 ± 0.01	21.0	83.8	4.89
50	1.12 ± 0.05	49.5	98.9	7.15
75	1.48 ± 0.01	75.3	100	1.55
100	1.83 ± 0.06	100	100	4.44
Undiluted sera [β-1,4-GalT-V] (pM)	ΔR_{ct} (kΩ)	Recovered [β-1,4-GalT-V] (pM)	Recovery (%)	RSD (n = 3) (%)
Blank	0.12 ± 0.01	N.D		
25	0.67 ± 0.01	24.8	99.9	1.69
50	1.02 ± 0.04	50.1	100	5.73
75	1.31 ± 0.11	72.7	96.9	6.11
100	1.64 ± 0.05	94.1	94.1	3.82

[a] 2.5, 5.0, 7.5, and 1.0 nM spiked sera were diluted 1:100 to obtain 25, 50, 75, and 100 pM solutions, respectively. ND: Non detected.

The feasibility of straightforward protein detection was assessed, and the results compared with those from the pretreatment protocol to simplify the measurement. The β-1,4-GalT-V glycoprotein concentration in human serum determined by EIS showed an RSD lower than 8% and 7% in diluted and undiluted samples, respectively. The high recovery of the β-1,4-GalT-V glycoprotein in human serum could be attributed to the antifouling properties of the mixed SAM onto the SPAuE surface. SAM's terminal hydroxyl groups form hydrogen bonds in contact with the aqueous samples, effectively counteracting the adsorption of matrix proteins [67,68]. The mixed SAM also allows tuning the distance among contiguous immobilized anti-β-1,4-GalT-V antibodies, preventing two neighboring antibodies from hindering each other in binding the β-1,4-GalT-V glycoprotein, thus increasing the glycoprotein recognition [69,70]. The β-1,4-GalT-V glycoprotein recovery assay using undiluted serum demonstrated that our immunosensor detects levels of the protein of clinical relevance straightforwardly and with fast response. It holds the potential for differentiation between healthy individuals and patients suffering CRC at the point-of-care. Furthermore, the immunosensor could also be applied to detect other glycoproteins associated with other diseases.

4. Conclusions

We successfully developed a label-free electrochemical immunosensor to detect the β-1,4-GalT-V CRC biomarker. The biosensing interface was developed by forming a mixed SAM of alkanethiols onto the SPAuE surface, with pending carboxylic acids covalently linking an anti-β-1,4-GalT-V antibody on the SPAuE surface. The anti-β-1,4-GalT-V antibody captured the β-1,4-GalT-V glycoprotein with high specificity,

detected by the sensitive EIS technique at low glycoprotein concentrations. The high performance of the electrochemical immunosensor allowed us to detect glycoprotein concentrations of clinical relevance in spiked serum samples and thus demonstrate the potential to determine the positive serostatus of CRC patients. Moreover, by their attributes as simplicity and low LOD, the electrochemical immunosensor reported herein offers new opportunities for diagnosis in decentralized settings.

Credit author statement

Danilo Echeverri: Conceptualization, Methodology, Writing – original draft, Research, Data curation, Formal analysis. **Jahir Orozco**: Conceptualization, Formal analysis, Funding acquisition, Project administration, Editing drafts and Supervision.

Declaration of competing interest

The authors declare that they have no known competing financial interests or personal relationships that could have appeared to influence the work reported in this paper.

Acknowledgments

The work has been funded by MINCIENCIAS, MINEDUCACIÓN, MINCIT and ICETEX through the Program Ecosistema Científico Cod. FP44842-211-2018, project number 58536. J. O thanks support from The University of Antioquia and the Max Planck Society through the cooperation agreement 566–1, 2014. We thank The Ruta N complex for hosting the Max Planck Tandem Groups.

Appendix A. Supplementary data

Supplementary data to this article can be found online at https://doi.org/10.1016/j.talanta.2022.123337.

References

[1] S.B. Chatterjee, J. Hou, V.V. Ratnam Bandaru, M.K. Pezhouh, A.A. Syed Rifat Mannan, R. Sharma, Lactosylceramide synthase β-1,4-GalT-V: a novel target for the diagnosis and therapy of human colorectal cancer, Biochem. Biophys. Res. Commun. (2019) 380–386, https://doi.org/10.1016/j.bbrc.2018.11.149.

[2] S. Chatterjee, A. Kolmakova, M. Rajesh, Regulation of lactosylceramide synthase (glucosylceramide β-1,4-galactosyltransferase); implication as A drug target, Curr. Drug Targets 9 (2008) 272–281, https://doi.org/10.2174/138945008783954952.

[3] K. Shirane, T. Sato, K. Segawa, K. Furukawa, Involvement of β-1,4-galactosyltransferase V in malignant transformation-associated changes in glycosylation, Biochem. Biophys. Res. Commun. 265 (1999) 434–438, https://doi.org/10.1006/bbrc.1999.1684.

[4] S.S. Pinho, C.A. Reis, Glycosylation in cancer: mechanisms and clinical implications, Nat. Rev. Cancer 15 (2015) 540–555, https://doi.org/10.1038/nrc3982.

[5] A. Seko, F. Kataoka, D. Aoki, M. Sakamoto, T. Nakamura, M. Hatae, S. Yonezawa, K. Yamashita, β1,3-Galactosyltransferases-4/5 are novel tumor markers for gynecological cancers, Tumor Biol. 30 (2009) 43–50, https://doi.org/10.1159/000203129.

[6] T. Asao, H. Kuwano, J.I. Nakamura, A. Okamura, E.G. Berger, K.L. Matta, S. Yazawa, Tumor cells as the origin of elevated serum α1,3fucosyltransferase in association with malignancy, Clin. Exp. Metastasis 18 (2000) 605–610, https://doi.org/10.1023/A:1011967119736.

[7] P. Geßner, S. Riedl, A. Quentmaier, W. Kemmner, Enhanced activity of CMP-NeuAc:Galβ1-4GlcNAc:α2,6-sialyltransferase in metastasizing human colorectal tumor tissue and serum of tumor patients, Cancer Lett. 75 (1993) 143–149.

[8] C. Fernández-Ponce, N. Geribaldi-Doldán, I. Sánchez-Gomar, R.N. Quiroz, L. A. Ibarra, L.G. Escorcia, R. Fernández-Cisnal, G.A. Martinez, F. García-Cózar, E. N. Quiroz, The role of glycosyltransferases in colorectal cancer, Int. J. Mol. Sci. 22 (2021) 1–20, https://doi.org/10.3390/ijms22115822.

[9] D. Bedja, W. Yan, V. Lad, D. Iocco, N. Sivakumar, V.V.R. Bandaru, S. Chatterjee, Inhibition of glycosphingolipid synthesis reverses skin inflammation and hair loss in ApoE−/− mice fed western diet, Sci. Rep. 8 (2018) 1–11, https://doi.org/10.1038/s41598-018-28663-9.

[10] S. Pan, R. Chen, R. Aebersold, T.A. Brentnall, Mass spectrometry based glycoproteomics - from a proteomics perspective, Mol. Cell. Proteomics 10 (2011) 1–14, https://doi.org/10.1074/mcp.R110.003251.

[11] C.H. Lin, C.W. Lin, K.H. Khoo, Proteomic identification of specific glycosyltransferases functionally implicated for the biosynthesis of a targeted glyco-epitope, Proteomics 8 (2008) 475–483, https://doi.org/10.1002/pmic.200700710.

[12] S. Hosseini, P. Vázquez-Villegas, M. Rito-Palomares, S.O. Martinez-Chapa, Advantages , disadvantages and modifications of conventional ELISA, in: Enzym. Immunosorbent Assay, SpringerBriefs in Applied Sciences and Technology, 2018, pp. 67–115. Singapore.

[13] Y. Kinoshita, T. Uo, S. Jayadev, G.A. Garden, T.P. Conrads, T.D. Veenstra, R. S. Morrison, Potential applications and limitations of proteomics in the study of neurological disease, Arch. Neurol. 63 (2006) 1692–1696, https://doi.org/10.1001/archneur.63.12.1692.

[14] D.K. Podolsky, K.J. Isselbacher, Characterization of monoclonal antibodies to serum galactosyltransferase, Proc. Natl. Acad. Sci. U.S.A. 81 (1984) 2529, https://doi.org/10.1073/PNAS.81.8.2529.

[15] E.T.S.G. da Silva, D.E.P. Souto, J.T.C. Barragan, J. de F. Giarola, A.C.M. de Moraes, L.T. Kubota, Electrochemical biosensors in point-of-care devices: recent advances and future trends, Chemelectrochem 4 (2017) 778–794, https://doi.org/10.1002/celc.201600758.

[16] S. Campuzano, R. Barderas, P. Yáñez-Sedeño, J.M. Pingarrón, Electrochemical biosensing to assist multiomics analysis in precision medicine, Curr. Opin. Electrochem. 28 (2021) 100703, https://doi.org/10.1016/j.coelec.2021.100703.

[17] G. Vásquez, A. Rey, C. Rivera, C. Iregui, J. Orozco, Amperometric biosensor based on a single antibody of dual function for rapid detection of Streptococcus agalactiae, Biosens. Bioelectron. 87 (2017) 453–458, https://doi.org/10.1016/j.bios.2016.08.082.

[18] D. Alzate, S. Cajigas, S. Robledo, C. Muskus, J. Orozco, Genosensors for differential detection of Zika virus, Talanta 210 (2020) 120648, https://doi.org/10.1016/j.talanta.2019.120648.

[19] S. Wang, L. Zhang, S. Wan, S. Cansiz, C. Cui, Y. Liu, R. Cai, C.-Y. Hong, I.T. Teng, M. Shi, Y. Wu, Y. Dong, W. Tan, Aptasensor with expanded nucleotide using DNA nanotetrahedra for electrochemical detection of cancerous exosomes, ACS Nano 11 (2017) 3943–3949, https://doi.org/10.1021/acsnano.7b00373.

[20] D. Echeverri, M. Garg, D. Varón Silva, J. Orozco, Phosphoglycan-sensitized platform for specific detection of anti-glycan IgG and IgM antibodies in serum, Talanta 217 (2020) 121117, https://doi.org/10.1016/j.talanta.2020.121117.

[21] J.H. Kim, C.H. Cho, M.Y. Ryu, J.-G. Kim, S.-J. Lee, T.J. Park, J.P. Park, Development of peptide biosensor for the detection of dengue fever biomarker, nonstructural 1, PLoS One 14 (2019), e0222144, https://doi.org/10.1371/journal.pone.0222144.

[22] S. Campuzano, M. Pedrero, P. Yáñez-Sedeño, J.M. Pingarrón, New challenges in point of care electrochemical detection of clinical biomarkers, Sensor. Actuator. B Chem. 345 (2021), https://doi.org/10.1016/j.snb.2021.130349.

[23] V. Pinkova Gajdosova, L. Lorencova, A. Blsakova, P. Kasak, T. Bertok, J. Tkac, Challenges for impedimetric affinity sensors targeting protein detection, Curr. Opin. Electrochem. 28 (2021) 100717, https://doi.org/10.1016/j.coelec.2021.100717.

[24] T. Kremers, N. Menzel, F. Freitag, D. Laaf, V. Heine, L. Elling, U. Schnakenberg, Electrochemical impedance spectroscopy using interdigitated gold–polypyrrole electrode combination, Phys. Status Solidi Appl. Mater. Sci. 217 (2020) 1900827, https://doi.org/10.1002/pssa.201900827.

[25] T. Bertok, P. Gemeiner, M. Mikula, P. Gemeiner, J. Tkac, Ultrasensitive impedimetric lectin based biosensor for glycoproteins containing sialic acid, Microchim. Acta 1801 (180) (2012) 151–159, https://doi.org/10.1007/S00604-012-0902-6.

[26] T. Bertok, A. Sediva, J. Katrlik, P. Gemeiner, M. Mikula, M. Nosko, J. Tkac, Label-free detection of glycoproteins by the lectin biosensor down to attomolar level using gold nanoparticles, Talanta 108 (2013) 11–18, https://doi.org/10.1016/j.talanta.2013.02.052.

[27] T. Bryan, X. Luo, P.R. Bueno, J.J. Davis, An optimised electrochemical biosensor for the label-free detection of C-reactive protein in blood, Biosens. Bioelectron. 39 (2013) 94–98, https://doi.org/10.1016/j.bios.2012.06.051.

[28] F.C.B. Fernandes, A. Santos, D.C. Martins, M.S. Góes, P.R. Bueno, Comparing label free electrochemical impedimetric and capacitive biosensing architectures, Biosens. Bioelectron. 57 (2014) 96–102, https://doi.org/10.1016/j.bios.2014.01.044.

[29] B.L. Garrote, A. Santos, P.R. Bueno, Perspectives on and precautions for the uses of electric spectroscopic methods in label-free biosensing applications, ACS Sens. 4 (2019) 2216–2227, https://doi.org/10.1021/acssensors.9b01177.

[30] D. Pihíková, P. Kasák, J. Tkac, Glycoprofiling of cancer biomarkers: label-free electrochemical lectin-based biosensors, Open Chem 13 (2015) 636–655, https://doi.org/10.1515/chem-2015-0082.

[31] A. Hushegyi, J. Tkac, Are glycan biosensors an alternative to glycan microarrays? Anal. Methods 6 (2014) 6610–6620, https://doi.org/10.1039/c4ay00692e.

[32] Y. Li, H.J. Schluesener, S. Xu, Gold nanoparticle-based biosensors, Gold Bull. 43 (2010) 29–41, https://doi.org/10.1007/BF03214964.

[33] B.L. Garrote, A. Santos, P.R. Bueno, Label-free capacitive assaying of biomarkers for molecular diagnostics, Nat. Protoc. 1512 (15) (2020) 3879–3893, https://doi.org/10.1038/s41596-020-0390-9.

[34] D. Nidzworski, K. Siuzdak, P. Niedziałkowski, R. Bogdanowicz, M. Sobaszek, J. Ryl, P. Weiher, M. Sawczak, E. Wnuk, W.A. Goddard, A. Jaramillo-Botero, T. Ossowski, A rapid-response ultrasensitive biosensor for influenza virus detection using antibody modified boron-doped diamond, Sci. Rep. 71 (7) (2017) 1–10, https://doi.org/10.1038/s41598-017-15806-7.

[35] W. Białobrzeska, D. Firganek, M. Czerkies, T. Lipniacki, M. Skwarecka, K. Dziąbowska, Z. Cebula, N. Malinowska, D. Bigus, E. Bięga, K. Pyrć, K. Pala, S. Żołędowska, D. Nidzworski, Electrochemical immunosensors based on screen-printed gold and glassy carbon electrodes: comparison of performance for

respiratory syncytial virus detection, Biosensors 10 (2020) 1–13, https://doi.org/10.3390/bios10110175.
[36] G. Dutta, F.C.B. Fernandes, P. Estrela, D. Moschou, P.R. Bueno, Impact of surface roughness on the self-assembling of molecular films onto gold electrodes for label-free biosensing applications, Electrochim. Acta 378 (2021) 138137, https://doi.org/10.1016/j.electacta.2021.138137.
[37] J.J. Gooding, S. Ciampi, The molecular level modification of surfaces: from self-assembled monolayers to complex molecular assemblies, Chem. Soc. Rev. 40 (2011) 2704–2718, https://doi.org/10.1039/C0CS00139B.
[38] P.A. Raymundo-Pereira, R. De Oliveira Pedro, O. Carr, M.E. Melendez, A.L. Gobbi, M. Helena De Oliveira Piazzetta, A.L. Carvalho, R.M. Reis, P.B. Miranda, O. N. Oliveira, Influence of the molecular orientation and ionization of self-assembled monolayers in biosensors: application to genosensors of prostate cancer antigen 3, J. Phys. Chem. C 125 (2021) 498–506, https://doi.org/10.1021/acs.jpcc.0c09055.
[39] J. Tkac, J.J. Davis, An optimised electrode pre-treatment for SAM formation on polycrystalline gold, J. Electroanal. Chem. 621 (2008) 117–120, https://doi.org/10.1016/j.jelechem.2008.04.010.
[40] A.N. Sekretaryova, M.Y. Vagin, A.V. Volkov, I.V. Zozoulenko, M. Eriksson, Evaluation of the electrochemically active surface area of microelectrodes by capacitive and faradaic currents, Chemelectrochem 6 (2019) 4411–4417, https://doi.org/10.1002/celc.201900989.
[41] D. Soto, M. Alzate, J. Gallego, J. Orozco, Electroanalysis of an Iron@Graphene-carbon nanotube hybrid material, Electroanalysis 30 (2018) 1521–1528, https://doi.org/10.1002/elan.201800115.
[42] S.P. Zankowski, P.M. Vereecken, Electrochemical determination of porosity and surface area of thin films of interconnected nickel nanowires, J. Electrochem. Soc. 166 (2019) D227–D235, https://doi.org/10.1149/2.0311906jes.
[43] T.A. Benites, W.C. Ribeiro, M.S. Góes, A.A.P. Ferreira, P.R. Bueno, Efeitos da rugosidade superficial nas propriedades de passivação de monocamadas orgânicas automontadas, Quim. Nova 37 (2014) 1533–1537, https://doi.org/10.5935/0100-4042.20140241.
[44] P. Bhadra, M.S. Shajahan, E. Bhattacharya, A. Chadha, Studies on varying n-alkanethiol chain lengths on a gold coated surface and their effect on antibody-antigen binding efficiency, RSC Adv. 5 (2015) 80480–80487, https://doi.org/10.1039/c5ra11725a.
[45] L. Liu, D. Deng, Y. Xing, S. Li, B. Yuan, J. Chen, N. Xia, Activity analysis of the carbodiimide-mediated amine coupling reaction on self-assembled monolayers by cyclic voltammetry, Electrochim. Acta 89 (2013) 616–622, https://doi.org/10.1016/j.electacta.2012.11.049.
[46] C. Ocaña, A. Hayat, R.K. Mishra, A. Vasilescu, M. del Valle, J.L. Marty, Label free aptasensor for Lysozyme detection: a comparison of the analytical performance of two aptamers, Bioelectrochemistry 105 (2015) 72–77, https://doi.org/10.1016/j.bioelechem.2015.05.009.
[47] T. Bertok, L. Lorencova, E. Chocholova, E. Jane, A. Vikartovska, P. Kasak, J. Tkac, Electrochemical impedance spectroscopy based biosensors: mechanistic principles, analytical examples and challenges towards commercialization for assays of protein cancer biomarkers, Chemelectrochem 6 (2019) 989–1003, https://doi.org/10.1002/celc.201800848.
[48] P. Córdoba-Torres, T.J. Mesquita, R.P. Nogueira, Relationship between the origin of constant-phase element behavior in electrochemical impedance spectroscopy and electrode surface structure, J. Phys. Chem. C 119 (2015) 4136–4147, https://doi.org/10.1021/jp512063f.
[49] P. Kanyong, A. V Patil, J.J. Davis, Annual review of analytical chemistry functional molecular interfaces for impedance-based diagnostics, Annu. Rev. Anal. Chem. 13 (2020) 183–200, https://doi.org/10.1146/annurev-anchem-061318-.
[50] A.H. Loo, A. Bonanni, A. Ambrosi, H.L. Poh, M. Pumera, Impedimetric immunoglobulin G immunosensor based on chemically modified graphenes, Nanoscale 4 (2012) 921–925, https://doi.org/10.1039/c2nr11492e.
[51] A. Pal, S. Biswas, S.P. O Kare, P. Biswas, S.K. Jana, S. Das, K. Chaudhury, Development of an impedimetric immunosensor for machine learning-based detection of endometriosis: a proof of concept, Sensor. Actuator. B Chem. 346 (2021) 130460, https://doi.org/10.1016/j.snb.2021.130460.
[52] L. Farzin, S. Sadjadi, M. Shamsipur, S. Sheibani, An immunosensing device based on inhibition of mediator's faradaic process for early diagnosis of prostate cancer using bifunctional nanoplatform reinforced by carbon nanotube, J. Pharm. Biomed. Anal. 172 (2019) 259–267, https://doi.org/10.1016/j.jpba.2019.05.008.
[53] C. Zhu, G. Yang, H. Li, D. Du, Y. Lin, Electrochemical sensors and biosensors based on nanomaterials and nanostructures, Anal. Chem. 87 (2014) 230–249, https://doi.org/10.1021/AC5039863.
[54] O.A. Sadik, H. Xu, E. Gheorghiu, D. Andreescu, C. Balut, M. Gheorghiu, D. Bratu, Differential impedance spectroscopy for monitoring protein immobilization and antibody-antigen reactions, Anal. Chem. 74 (2002) 3142–3150, https://doi.org/10.1021/ac0156722.
[55] J. Quinchia, D. Echeverri, A.F. Cruz-Pacheco, M.E. Maldonado, J. Orozco, Electrochemical biosensors for determination of colorectal tumor biomarkers, Micromachines 11 (2020) 411, https://doi.org/10.3390/MI11040411.
[56] H.W. Schroeder, L. Cavacini, Structure and function of immunoglobulins, J. Allergy Clin. Immunol. 125 (2010) S41, https://doi.org/10.1016/j.jaci.2009.09.046.
[57] A.R. Temming, A.E.H. Bentlage, S.W. de Taeye, G.P. Bosman, S.N. Lissenberg-Thunnissen, N.I.L. Derksen, G. Brasser, J.Y. Mok, W.J.E. van Esch, H.L. Howie, J. C. Zimring, G. Vidarsson, Cross-reactivity of mouse IgG subclasses to human Fc gamma receptors: antibody deglycosylation only eliminates IgG2b binding, Mol. Immunol. 127 (2020) 79–86, https://doi.org/10.1016/j.molimm.2020.08.015.
[58] J. Orozco, C. Jiménez-Jorquera, C. Fernández-Sánchez, Gold nanoparticle-modified ultramicroelectrode arrays for biosensing: a comparative assessment, Bioelectrochemistry 75 (2009) 176–181, https://doi.org/10.1016/j.bioelechem.2009.03.013.
[59] J.A. Goode, J.V.H. Rushworth, P.A. Millner, Biosensor regeneration: a review of common techniques and outcomes, Langmuir 31 (2015) 6267–6276, https://doi.org/10.1021/la503533g.
[60] N.T. Flynn, T.N.T. Tran, M.J. Cima, R. Langer, Long-term stability of self-assembled monolayers in biological media, Langmuir 19 (2003) 10909–10915, https://doi.org/10.1021/LA035331E.
[61] M.K. Strulson, D.M. Johnson, J.A. Maurer, Increased stability of glycol-terminated self-assembled monolayers for long-term patterned cell culture, Langmuir 28 (2012) 4318–4324, https://doi.org/10.1021/la2035533.
[62] J.A. Jones, L.A. Qin, H. Meyerson, K.K. Il, T. Matsuda, J.M. Anderson, Instability of self-assembled monolayers as a model material system for macrophage/FBGC cellular behavior, J. Biomed. Mater. Res. 86 (2008) 261–268, https://doi.org/10.1002/jbm.a.31660.
[63] C.A. Scotchford, E. Cooper, G.J. Leggett, S. Downes, Growth of human osteoblast-like cells on alkanethiol on gold self- assembled monolayers: the effect of surface chemistry, J. Biomed. Mater. Res. 41 (1998) 431–442, https://doi.org/10.1002/(SICI)1097-4636(19980905)41:3<431::AID-JBM13>3.0.CO;2-L.
[64] T.P. Taylor, M.G. Janech, E.H. Slate, E.C. Lewis, J.M. Arthur, J.C. Oates, Overcoming the effects of matrix interference in the measurement of urine protein analytes, Biomark. Insights 7 (2012) 1, https://doi.org/10.4137/BMI.S8703.
[65] R.N. Fichorova, N. Richardson-Harman, M. Alfano, L. Belec, C. Carbonneil, S. Chen, L. Cosentino, K. Curtis, C.S. Dezzutti, B. Donoval, G.F. Doncel, M. Donaghay, J.C. Grivel, E. Guzman, M. Hayes, B. Herold, S. Hillier, C. Lackman-Smith, A. Landay, L. Margolis, K.H. Mayer, J.M. Pasicznyk, M. Pallansch-Cokonis, G. Poli, P. Reichelderfer, P. Roberts, I. Rodriguez, H. Saidi, R.R. Sassi, R. Shattock, J.E. Cummins, Biological and technical variables affecting immunoassay recovery of cytokines from human serum and simulated vaginal fluid: a multicenter study, Anal. Chem. 80 (2008) 4741–4751, https://doi.org/10.1021/ac702628q.
[66] S.L. Moura, M. Martì, M.I. Pividori, Matrix effect in the isolation of breast cancer-derived nanovesicles by immunomagnetic separation and electrochemical immunosensing—a comparative study, Sensors 20 (2020) 965, https://doi.org/10.3390/S20040965.
[67] M. Drozd, S. Karoń, E. Malinowska, Recent advancements in receptor layer engineering for applications in SPR-based immunodiagnostics, Sensors 21 (2021) 3781, https://doi.org/10.3390/S21113781.
[68] T. Hayashi, M. Hara, Nonfouling self-assembled monolayers: mechanisms underlying protein and cell resistance, Curr. Phys. Chem. 1 (2011) 90–98, https://doi.org/10.2174/1877946811101020090.
[69] D. Blasi, L. Sarcina, A. Tricase, A. Stefanachi, F. Leonetti, D. Alberga, G. F. Mangiatordi, K. Manoli, G. Scamarcio, R.A. Picca, L. Torsi, Enhancing the sensitivity of biotinylated surfaces by tailoring the design of the mixed self-assembled monolayer synthesis, Cite This ACS Omega 5 (2020) 16762–16771, https://doi.org/10.1021/acsomega.0c01717.
[70] D.A. Sadık, H. Eksi-Kocak, G. Ertaş, İ.H. Boyacı, M. Mutlu, Mixed-monolayer of N-hydroxysuccinimide-terminated cross-linker and short alkanethiol to improve the efficiency of biomolecule binding for biosensing, Surf. Interface Anal. 50 (2018) 866–878, https://doi.org/10.1002/SIA.6489.